Old Dominion University

ODU Digital Commons

Electrical & Computer Engineering Theses & Dissertations

Electrical & Computer Engineering

Spring 2017

Deposition of Silicon Thin Films by Ion Beam Assisted Deposition

Tejaswini Miryala
Old Dominion University, tmiry001@odu.edu

Follow this and additional works at: https://digitalcommons.odu.edu/ece_etds

Part of the Power and Energy Commons

Recommended Citation

Miryala, Tejaswini. "Deposition of Silicon Thin Films by Ion Beam Assisted Deposition" (2017). Master of Science (MS), Thesis, Electrical & Computer Engineering, Old Dominion University, DOI: 10.25777/t8dq-6196
https://digitalcommons.odu.edu/ece_etds/19

This Thesis is brought to you for free and open access by the Electrical & Computer Engineering at ODU Digital Commons. It has been accepted for inclusion in Electrical & Computer Engineering Theses & Dissertations by an authorized administrator of ODU Digital Commons. For more information, please contact digitalcommons@odu.edu.

DEPOSITION OF SILICON THIN FILMS BY ION BEAM ASSISTED DEPOSITION

by

Tejaswini Miryala
B.Tech. May 2015, Jawaharlal Nehru Technological University, India

A Thesis Submitted to the Faculty of
Old Dominion University in Partial Fulfillment of the
Requirements for the Degree of

MASTER OF SCIENCE

ELECTRICAL AND COMPUTER ENGINEERING

OLD DOMINION UNIVERSITY
May 2017

Approved by:

Sylvain Marsillac (Director)

Christian Zemlin (Member)

Chung Hao Chen (Member)

ABSTRACT

DEPOSITION OF SILICON THIN FILM BY ION BEAM ASSISTED DEPOSITION

Tejaswini Miryala
Old Dominion University, 2017
Director: Dr. Sylvain Marsillac

With the depletion of non-renewable energy sources owing to increasing demands, we need to develop renewable energy sources, which can replace them with cleaner energy sources. The solar industry is one of these renewable energies. In spite of having very high potential, harvesting solar energy has been a challenge due to the cost of solar cells. Silicon dominates the photovoltaic industry, but even this technology can accommodate great improvements. This can be done notably by finding low cost deposition techniques for the silicon. The main aim of this thesis is to form high-quality nanocrystalline silicon thin films with the help of sputtering and ion beam deposition. Various characterization techniques were used to analyze the samples and demonstrate that ion beams indeed assist in obtaining higher quality nanocrystalline thin films.

Copyright, 2017, by Tejaswini Miryala, All Rights Reserved.

This thesis is dedicated to my parents, Prasadrao Miryala and Rajyalaxmi Miryala.

ACKNOWLEDGMENTS

First of all I express my whole hearted gratitude to Dr. Sylvian Marsillac, my research advisor for all his motivation and guidance during my research work as well as for giving me confidence to finish my future dissertation. I am extremely thankful for the knowledge and experience that I gained being a part of your research team.

I am grateful to Dr. Christian Zemlin, Associate Professor of the Department of Electrical and Computer Engineering, Old Dominion University and Dr. Chung Hao Chen, Assistant Professor of the Department of Electrical and Computer Engineering, Old Dominion University for their willingness to serve on my thesis committee and spending their valuable time for reviewing the thesis.

A special thanks goes to Dr. Dimitrie Popescu, Associate Professor, Graduate Program Director of the Electrical and Computer Engineering, Old Dominion University for his guidance on the course requirements and for his advice on academic matters.

A special thanks to all my research group members, Grace Rajan, Shankar Karki, Chinedum John Akwari, and Isaac Butt, for their support and the team experience they have offered me during my thesis work.

Last, but certainly not least, I would like to thank my parents, family, and friends for their continuous support and persistent belief in me not only during my Masters, but my entire life.

TABLE OF CONTENTS

Page

LIST OF FIGURES vii

Chapter

1. INTRODUCTION 1
   - 1.1 BACKGROUND 1
   - 1.2 THE ROLE OF SILICON THIN FILMS IN THE PV INDUSTRY 2
   - 1.3 THESIS OBJECTIVES AND ORGANIZATION 2
2. OVERVIEW OF SILICON TECHNOLOGY AND CHARACTERIZATION 4
   - 2.1 MONOCRYSTALLINE SILICON SOLAR CELLS 4
   - 2.2 POLY CRYSTALLINE SILICON SOLAR CELLS 5
   - 2.3 AMORPHOUS SILICON SOLAR CELLS 6
   - 2.4 CHARACTERIZATION 6
3. EFFECT OF SPUTTERING PROCESS PARAMETERS ON SILICON THIN FILMS GROWTH 13
   - 3.1 THE PHYSICS OF SPUTTERING 13
   - 3.2 SAMPLE PREPARATION 22
   - 3.3 EFFECT OF SUBSTRATE TEMPERATURE 23
   - 3.4 EFFECT OF SPUTTERING POWER 23
   - 3.5 EFFECT OF SUBSTRATES 26
   - 3.6 CONCLUSION 28
4. EFFECT OF ION BEAM ASSISTED DEPOSITION ON SILICON THIN FILMS GROWTH 29
   - 4.1 ION SOURCES 29
   - 4.2 THEORY OF OPERATION 30
   - 4.3 SAMPLE PREPARATION 34
   - 4.4 EFFECT OF ION BEAM PARAMETERS 35
   - 4.5 EFFECT OF SPUTTERING POWER 37
   - 4.6 CONCLUSION 39
5. SUMMARY 40
   - 5.1 SUMMARY 40
   - 5.2 FUTURE WORK 41

REFERENCES 42

VITA 44

LIST OF FIGURES

Figure Page

2.1 Experimental Setup for XRD 7

2.2 The principle of ellipsometry 8

2.3 Basic setup to measure the carrier concentration using a Hall effect [based on 11]. 10

2.4 Four point probe measurement setup…………………………………………...……12

3.1 The three primary regions of a gas discharge [based on 12] 14

3.2 Schematic of a sputter deposition system [based on 13] 17

3.3 Schematic of a planar magnetron arrangement [based on 13] 20

3.4 Schematic showing the principal arrangement of a RF sputtering system [based on 13] 22

3.5 Complex dielectric functions ε_1 and ε_2 extracted by spectroscopic ellipsometry as a function of substrate temperature for silicon thin films deposited on silicon wafers with native oxide. 23

3.6 XRD spectra of the deposited silicon film for different sputtering power 24

3.7 Influence of sputtering power on the electrical mobility of the silicon film. 25

3.8 Influence of sputtering power on electrical properties of the silicon films for different substrates 26

3.9 Complex dielectric function ε_2 extracted by spectroscopic ellipsometry for different substrates 27

3.10 XRD spectra of the deposited silicon film on different substrates 28

4.1 Schematic of an ion beam source [based on 18] 30

Figure Page

4.2. Schematic of the ion acceleration process [based on 18] 32

4.3 The electrical schematic for a filament DC source [based on 18] 34

4.4 Influence of ion beam on the optical properties of the sputtered silicon films extracted by spectroscopic ellipsometry 35

4.5 Influence of ion beam parameters on the mobility of the silicon films 36

4.6 Influence of ion beam parameters on the conductivity of the silicon films 36

4.7 Complex dielectric function spectra ε1 and ε2 of silicon films deposited with IBAD as a function of sputtering power 38

CHAPTER 1

INTRODUCTION

1.1 BACKGROUND

The rapid growth in the human population is causing rapid growth in energy demand and consumption today. The world energy market is dominated by the non-renewable energy sources. Due to limited sources, research has been done on renewable energy sources in which solar energy is more appealing. Solar energy conversion can be divided into two different technologies, *solar thermal* and *photovoltaics* (PV). In solar thermal, energy from sunlight is converted into heat for domestic use or for conversion to electricity in large sized, concentrated solar power plants, whereas, in PV, energy from sunlight is directly converted into DC electricity. Solar cells convert sun light into electricity using the photovoltaic effect. When sunlight falls on a semiconductor, electron-hole pairs are generated by absorbing the photon energy, which of course depends on the photon energy and band gap of the semiconductor. The photo-generated charge carriers can be extracted in the presence of an electric field across a pn junction, which is formed by contacting n-type and p-type semiconductors. The charge carrier dissipates their energy in the external circuit. In this way, the energy from the sun is directly converted into electricity by the solar cells.

Edmund Becquerel was the first to report the production of current and voltage illuminating a silver chloride electrode immersing in an electrolyte solution in 1839. In the year 1953, about 6% efficient silicon solar cells were developed at Bell Laboratory [1]. Since then, more efficient solar cells have been developed with the help of advanced knowledge in material processing and technology.

1.2 THE ROLE OF SILICON THIN FILMS IN THE PV INDUSTRY

In the present situation, photovoltaics are largely dominated by crystalline silicon (c-Si) and poly-crystalline silicon technologies. But thin film solar cells, including amorphous silicon, are also very attractive. This is mainly due to the cost reduction of the solar cells by using thin films. The active layers are usually deposited on a glass substrate. However, other substrates like stainless steel and plastics can also be used. Thin film silicon solar cells require less fabrication energy compared to the crystalline and poly-crystalline silicon fabrications. Thus, the energy payback time is generally reduced. Moreover, compared to the other thin film fabrications coming into existence, silicon thin films have an advantage since they are using silicon as a raw material, which is nontoxic and widely procurable. The problem of thin film silicon solar cells at present is their lower conversion efficiency compared to the crystalline silicon processing technologies and the difficulty of depositing them with high quality. The main challenge is lowering the manufacturing costs and the material dimensions as well as increasing material quality to meet growing energy demands.

1.3 THESIS OBJECTIVES AND ORGANIZATION

The aim of this thesis is to discover and develop a deposition process that allows for grain size enhancement in silicon thin films. In order to achieve this, several processes are considered, specifically magnetron sputtering and magnetron sputtering with Ion Beam Assisted Deposition (IBAD). Moreover, the effects of the deposition parameters of magnetron sputtering and IBAD on the thin film properties are studied and correlated with the properties of the films, with the goal of finding the appropriate deposition parameters.

In Chapter 2, an overview of silicon technology and the various characterization techniques (including XRD, spectroscopic ellipsometry (SE), Hall effect, and four point probe) used are presented.

In Chapter 3, an overview of sputtering deposition process and the various parameters like effect of sputtering power, the effects of substrates and the effect of substrate temperature on the silicon thin film properties are presented.

In Chapter 4, the deposition process using IBAD is discussed and different parameters like effect of IBAD parameters and sputtering power on deposition of the silicon thin film properties are presented.

Finally, Chapter 5 concludes the thesis and presents some potential future work.

CHAPTER 2

OVERVIEW OF SILICON TECHNOLOGY AND CHARACTERIZATION

2.1 MONOCRYSTALLINE SILICON SOLAR CELLS

Crystalline silicon solar cells dominate the photovoltaic (PV) technology market. The reason that crystalline silicon is dominant in photovoltaic (PV) technology is the fact that microelectronics has developed silicon technology very remarkably; however, the technology has to be cost effective to compete directly with other energy sources, such as fossil fuels. In most commercial arrays, PV cells, are fabricated from boron doped crystalline silicon (c-Si) sliced form Czochralski (CZ) ingots. The efficiency of these cells is more than 20% [2]. In the Czochralski method, pure silicon pieces are melted in a crucible and a seed crystal is first dipped into the melt. Then the seed is slowly removed vertically, allowing the liquid to crystallize, which matches the crystalline structure of the seed. A small amount of boron (B) is integrated for n-type doping during the crystal growth [3]. The silicon wafers are sliced from long cylindrical shape ingots, which are then cut and polished.

Basically, there are three different structures of high efficiency monocrystalline silicon solar cells namely, (a) the passivated emitter rear localized cell (PERL), (b) the heterojunction with intrinsic thin layer (HIT) cell and, (c) the back contact, back junction (BC-BJ) cell. A PERL type cell uses a p-type float zone (FZ) monocrystalline silicon substrate with front and rear surface passivation layers, an inverted-pyramid light trapping surface, and a rear localized p^+ layer, which provides the back surface field and a double layer of anti-reflective coating (ARC) [4]. In the case

of a HIT cell, a thin intrinsic amorphous layer is introduced between the p- and n-doped layer on either side of a randomly textured n-type CZ crystalline silicon wafer, forming a p/n heterojunction on p-side and obtaining a back surface field on n-side. The transparent conducting oxide and the electrodes are fabricated on both sides of the device [5]. BC-BJ type cells are formed by interdigitated n- and p- regions with no metallization on the front surface to shadow the incident photon which helps to generate high photo-generated current [6]. The low contact resistance of interconnection, which improves fill factor, is an additional benefit of this design.

2.2 POLY CRYSTALLINE SILICON SOLAR CELLS

Polycrystalline silicon ingots and wafers are cost effective compared to monocrystalline silicon. Among many others, the chemical and metallurgical processes are two ways to obtain solar grade polycrystalline silicon [7]. In the chemical process, solar-grade polycrystalline silicon is obtained from a chemical purification of silicon, known as a Siemens process, which involves decomposition of thrichlorosilane by chemical vapor deposition [7]. In the metallurgical process, solar-grade polycrystalline silicon is obtained directly from metallurgical silicon by a reduction of silicon in the presence of carbon [7].

The current record efficiency of a research polycrystalline silicon solar cell is 21.9%, which is about 3.5% lower than a monocrystalline silicon solar cell. The efficiency difference between mono- and polycrystalline silicon cells is attributable to the lower quality of polycrystalline silicon substrate which has a higher minority carrier recombination due to high impurity densities as well as crystal defects such as grain boundaries and dislocations. The high efficiency polycrystalline silicon cells are fabricated in a PERL structure [8]. A BC-BJ cell design without a front p-n junction, which requires a high quality substrate with high minority carrier lifetimes, may not be particularly suitable for polycrystalline silicon solar cells. However, the new types of back contacts

cells, such as a metal wrap through and an emitter wrap through, are preferable since the front p-n junction in these cells can provide a higher minority carrier collection [4].

2.3 AMORPHOUS SILICON SOLAR CELLS

Amorphous silicon (a-Si) cells are a non-crystalline form of silicone and are a cheap alternative to the crystalline silicon solar cells consisting of hydrogenated amorphous silicon. a-Si alloys have a high absorption coefficient due to internal scattering mechanism [9]. Amorphous silicon is difficult to be doped due to the presence of dangling bonds. By introducing hydrogen during the fabrication of a-Si, passivation of the defects occurs, which improves the photoconductivity and enhance doping. Amorphous silicon panels are deposited by a glow discharge technique with the help of plasma known as a Plasma Enhanced Chemical Vapor Deposition (PECVD). They can be also deposited at low temperatures.

a-Si solar cells have an efficiency of about 9% (14% in triple junction form), which is significantly lower than a crystalline silicon cell, whose efficiency is above 20%. The main drawback of amorphous silicon solar cells is the light induced degradation due to the Stabler-Wronski effect, which leads to the degradation of efficiency. The principle advantage of amorphous silicon solar cells is their manufacturing costs and also their ability to be deposited on a large area of flexible substrates. Amorphous silicon solar cells are lightweight and flexible, and can be molded into any size and shape, as there is no particular orientation of atomic structure.

2.4 CHARACTERIZATION

2.4.1 XRD

X-ray powder diffraction (XRD) is a rapid analytical technique primarily used for phase identification of a crystalline material and also to measure unit cell dimensions of thin film materials. The energetic x-rays can penetrate deep into the materials and provide information about

the grain structure. In general, X-rays are produced by either x-ray tubes or synchrotron radiation. In an x-ray tube, x-rays as primary source are generated when a focused electron beam accelerated across a high voltage field collides a stationary or rotating solid target. As electrons bombard with atoms in the target and slow down, a continuous spectrum of x-rays is emitted, which is referred to as Bremsstrahlung radiation. The electrons with high energy also eject electrons from inner shells through the ionization process. When a free electron fills the shell, a characteristic x-ray photon is emitted. XRD allows extracting lattice constant, average grain size, preferential rientation of the grains and strain in the lattice.

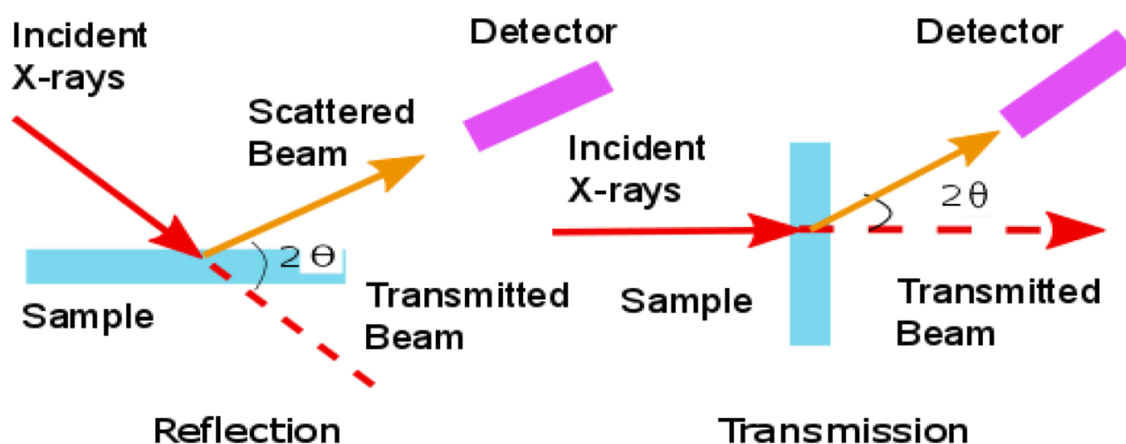

Fig. 2.1 Experimental Setup for XRD

A Miniflex II Benchtop X-Ray Diffractometer (Rigaku), which is a scintillation counter, was used for all XRD measurements in this thesis. As shown in Figure 2.1, when a beam of x-rays interacts with a crystal, it is diffracted from the crystalline phase according to Bragg's Law (λ=2d sinθ). The intensity of the diffracted x-ray is plotted with respect to the diffracted angle. Peaks are

observed when the Bragg's Law is satisfied. Comparing the peaks with the XRD data on powdered samples helps to determine the lattice constants and crystal orientation.

2.4.2 SPECTROSCOPIC ELLIPSOMETRY (SE) MEASUREMENT

Ellipsometry is a non-destructive optical characterization technique for measuring thin film materials properties. Spectroscopic ellipsometry is used to characterize the optical properties of thin film and bulk materials. Regardless of the material used, this characterization technique is ideal for the measurement of the film thickness and optical constants. It relies on the polarization change caused by reflection or transmission from a material structure (Figure 2.2).

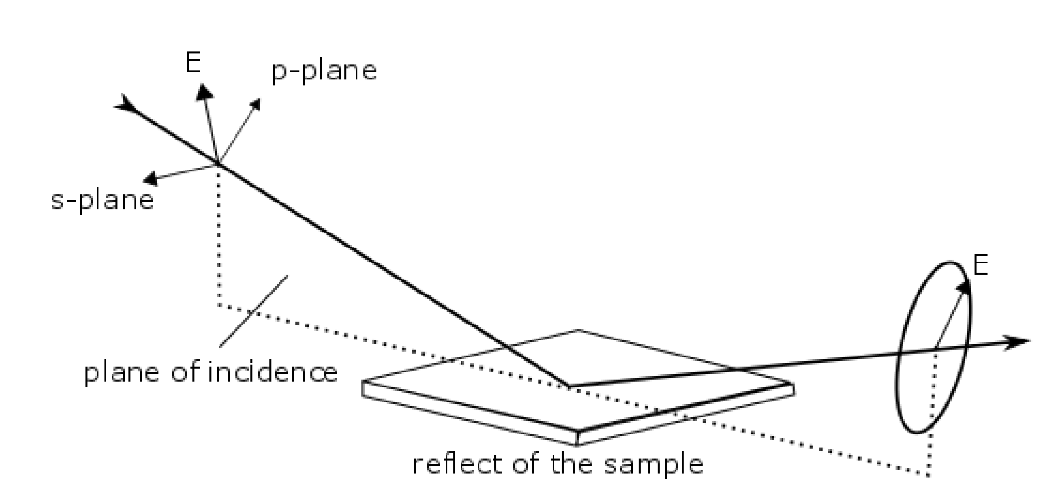

Fig. 2.2 The principle of ellipsometry

The main tools used for collecting ellipsometry data includes a light source, a polarization generator, a sample, a polarization analyzer and a detector. The monochromatic light source is obtained using a laser, by using an arc lamp or by using a polychromatic source and filtering. The polarization generator and analyzer are optical components used to manipulate the polarization. A polarization generator is used to convert the unpolarized light to linearly polarized light whereas a

polarization analyzer converts the elliptically polarized light to linearly polarized light. The detector is used to measure the light intensity. The different ellipsometer configurations include a rotating analyzer ellipsometer (RAE), a rotating polarizer (RPE), a rotating compensator (RCE), and a phase modulation (PME) [10]. The rotating analyzer ellipsometer configuration uses a polarizer to define the incoming polarization and then a rotating analyzer is used to analyze the outgoing light from the sample. The polarizer allows the passage of light of a preferred electric field orientation. The axis of the polarizer is oriented between the parallel and perpendicular plane such that the light falls directly on the sample. The linearly polarized light gets reflected from the sample surface as elliptically polarized light and it is passed through a rotating analyzer ellipsometer. In some configurations, a rotating compensator is used to shift the relative phase of orthogonal vector components resolved along the fast and slow axes of the compensator. The phase shift between the p and s components of the electric field vector depends on the angle of the fast axis of the compensator with respect to the field of incidence. The light beam reflects from the sample surface thus inducing a change in the nature of the polarization state modulation. Upon specular reflection, the beams pass through a polarization analyzer and are collected by the spectograph. The detector converts the light to voltage and helps in in determining the reflected polarization. These data are used to compare the input and reflected polarization of the sample. After the measurment, an optical model is constructed coresponding to the sample, with respect to the sample structure of known component materials. The thickness of the film and the optical constants are determined by the interference between the light travelling through the film and the light reflected from the surface.

2.4.3 HALL EFFECT

The carrier concentration is different for different type of semiconductor materials. To measure such a carrier concentration, one can use a Hall effect measurement. It is also possible to measure the carrier type directly, allowing to distinguish whether the majority carriers are holes or electrons. A Hall measurement can be performed to determine the resistivity, free electron, and electron mobility. First, in order to prepare a sample for measurement, on the four edges of the thin film solar cell, an aluminum conductive paste is coated and placed on a sample holder with connections of electrical probes from the four corners of the sample. Then by using a Van der Pauw configuration, the Hall measurements are made. The sample holder is placed in a magnetic field generated between two parallel coils. The basic setup for a Hall effect is shown in Fig. 2.3[11].

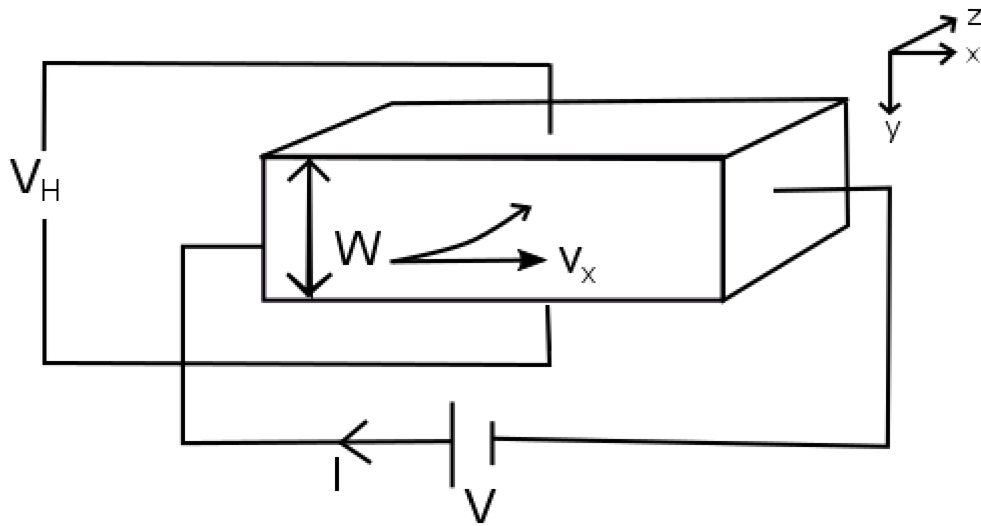

Fig. 2.3 Basic setup to measure the carrier concentration using a Hall effect [based on 11].

Consider a p-type material with a voltage V applied along the length. The carriers will have then a velocity v_x along the x-axis due the difference of potential. We then apply a magnetic field

along the z-direction, B_z. A Lorentz force, qv_xB_z, is then felt by the holes flowing in the x-direction. The holes accumulate at the top due to the upward Lorentz force, which give rise to a downward electric field E_y. Since there is no current flow in the y-axis direction it balances the Lorentz force exactly, so that:

$$qE_y = qv_xB_z \qquad (2.0)$$

The establishment of this electric field is known as the Hall effect. By considering hole drift velocity, the hall field E_y is

$$E_y = \left[\frac{J_p}{qp}\right]B_z = R_H E J_p B_z \qquad (2.2)$$

$$R_H = \frac{1}{qp} \qquad (2.3)$$

where R_H is the hall coefficient. For n-type materials, the Hall coefficient is negative.

2.4.4 FOUR POINT PROBE

The sheet resistances measured in this thesis have been measured using a four point probe setup and then compared with the Hall effect. A four point probe is an instrument for measuring the resistivity of semiconductor devices, which is used to calculate the doping concentrations. It can measure both bulk and thin film specimens. The experiment is as shown in Figure 2.4.

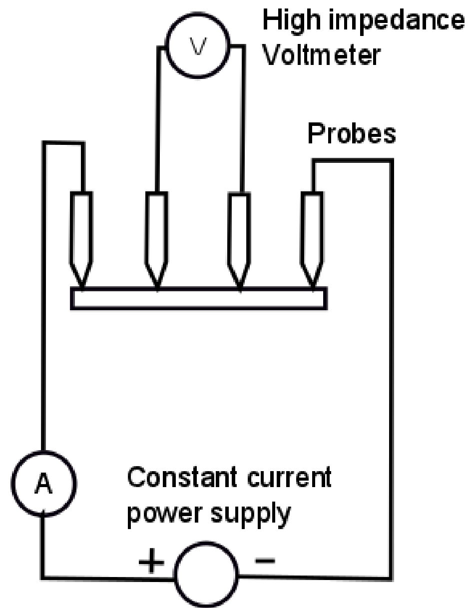

Fig. 2.4 Four point probe measurement setup

In a four point probe measurement, the four probes are aligned parallel at a fixed distance and a current runs through the outer probes and voltage is measured between the inner probes. From the measured voltage and the current applied, we can calculate the sheet resistance using

$$\rho\left(\frac{\Omega}{sq}\right) = \frac{\pi}{\ln(2)}\frac{V}{I} \tag{2.5}$$

where,

I = current flowing through the outer probes

V = potential difference between inner probes in volts.

CHAPTER 3

EFFECT OF SPUTTERING PROCESS PARAMETERS ON SILICON THIN FILMS GROWTH

3.1 THE PHYSICS OF SPUTTERING

The most conventional process of sputtering is plasma based sputtering where plasma is present and positive ions are accelerated towards the target, which is at a negative potential. The plasma-based sputter deposition can be described using a simple experimental setup. A cathode and an anode are placed opposite to each other in a vacuum chamber, which is pumped down by a combination of turbo molecular and rotary pumps to a base pressure of 10^{-6} or 10^{-7} Torr. A noble gas, usually argon, is allowed into the chamber to raise the chamber pressure to 10^{-3} Torr. When a high voltage difference is applied between the cathode and anode, a glow discharge is ignited. The I-V characteristic of the discharge is illustrated in Fig. 3.1. Three general regions, the dark discharge region, the glow discharge and the arc discharge can be identified in the Fig 3.1. The dark discharge region is between A and E in the figure and refers to the region where the discharge remains invisible to the eye. In this region, the ions and electrons formed by background ionization move in the direction of electrodes due to the applied electrical field, thereby producing a weak electrical current. As the voltage increased, a larger portion of ions and electrons will reach the electrode.

Even with the increase in voltage, the current remains constant in the region between B and C. Later, as the voltage is increased gradually we notice the increase of current. This increase in current is illustrated between regions C – E. This increase in current can be accounted by the impact of ionization of atoms by the original electrons escalated across the electric field. Hence,

an avalanche of ions and electrons production will follow, leading to a strong increase in current. This region is referred to as Townsend discharge. The corona discharges are glow discharges and are visible to the eye, they are observed at higher currents. Corona discharges (D – E) occur in Townsend dark discharges, prior to electrical breakdown, in regions of high electric field near the sharp points. The electrical breakdown takes place at a higher electrical field due to the emission of additional secondary electrons. Thus at the breakdown potential (point E), the current may increase remarkably and is limited by the internal resistance of the power supply connected between the plates. If the internal resistance is low, then the gas will breakdown at the indicated voltage and move into the normal discharge region (region F – G).

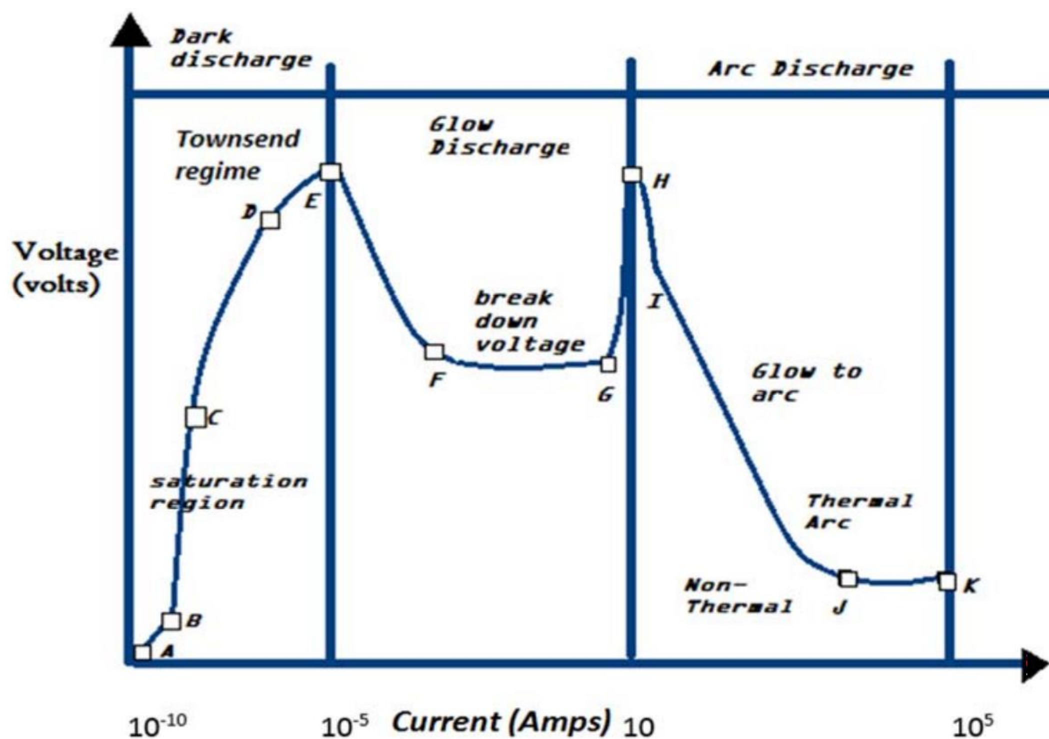

Fig. 3.1 The three primary regions of a gas discharge [based on 12]

Even with the increase in voltage, the current remains constant in the region between B and C. Later, as the voltage is increased gradually we notice the increase of current. This increase in current is illustrated between regions C – E. This increase in current can be accounted for by the impact of ionization of atoms by the original electrons escalated across the electric field. Hence, an avalanche of ions and electrons production will follow, leading to a strong increase in current. This region is referred to as a Townsend discharge. The corona discharges are glow discharges and are visible to the eye, they are observed at higher currents. Corona discharges (D – E) occur in Townsend dark discharges, prior to electrical breakdown, in regions of high electric field near the sharp points. The electrical breakdown takes place at a higher electrical field due to the emission of additional secondary electrons. Thus at the breakdown potential (point E), the current may increase remarkably and is limited by the internal resistance of the power supply connected between the plates. If the internal resistance is low, then the gas will breakdown at the indicated voltage and move into the normal discharge region (region F –G)[12].

3.1.1 SPUTTERING YIELD

Sputtering yield is a significant parameter, which is used to characterize the process of sputtering. It is defined as the removal rate of surface atoms due to ion bombardment, i.e. the mean number of atoms removed from the surface of a solid per incident ion and is given by [13]

$$S = \frac{number\ of\ emitted\ particles}{number\ of\ incident\ ions} \tag{3.1}$$

For the yield calculation, the number of atoms that actually rise up to the surface is calculated and then the atoms with sufficient energy to break the surface binding forces are selected. However, it also requires the amount of energy deposited by the particles near the surface to be calculated. The energy of the incident particles and the incident angle plays a vital role in sputter yield.

Sputter deposition is a widely used technique for the deposition of thin films. In the basic process, the target plate is bombarded with the high energy ions, which are produced in the presence of plasma. The collision process causes removal of the target atoms from the surface of the target resulting in thin layer deposition on the substrate. Moreover, not only the ions but electrons are also ejected from the target and they play a crucial role in maintaining the plasma. The ejected atoms from the surface of the target during the sputtering process can be used to deposit on the selected substrate. In this process, the atoms eject from the surface with high energy. Thus, it results from collisions between the incident energized particles with surface atoms. Each individual atom acquires the required amount of energy as the momentum of the incident ion is transferred to the target ions during the collision process, which helps the atoms to eject from the surface. The ions undergo a series of collisions in the target. The process of sputtering can be classified into four different steps: (1) plasma ignition, (2) ion bombardment, (3) sputtered atom transfer and (4) film growth [14]. Fig 3.2 shows the schematic of a sputtering deposition system.

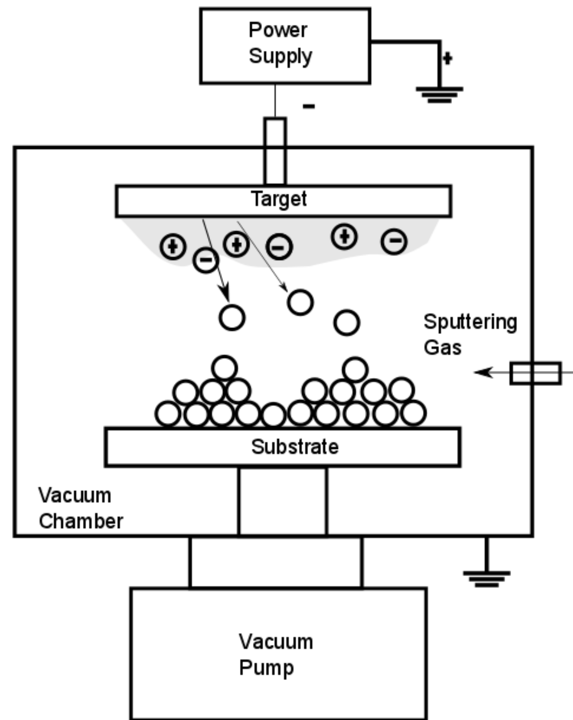

Fig. 3.2 Schematic of a sputter deposition system [based on 13]

1. Plasma ignition

When an electric field is applied between two electrodes and any electron present is accelerated towards the cathode with sufficient amount of energy to ionize gas atoms upon collision and produce a glow discharge. This creates an avalanche effect that helps in generation of more electrons to ionize the gas and create a plasma. Thus, these positively charged ions created in the plasma are accelerated towards the target leading to sputtering of the material.

2. Ion bombardment

The positive charged ions in the plasma transfer their momentum to the target material and disrupt the target surface. When two atoms collide simultaneously, most of the energy is transported to the primary atom and a portion is transferred to the secondary atom. The primary atom creates a series of collisions in the surrounding atoms while the secondary atom transfers its energy to the surrounding atoms causing them to eject. The collision process entirely depends on the mass of the incident ion. The surrounding atoms are involved in the energy exchange between incident ions and surface atoms of the target. From the Law of Conservation of Momentum and Energy, E_t transferred by collision is given by:

$$\frac{E_t}{E_i} = \frac{4M_t M_i cos^2\theta}{(M_t + M_i)^2} \tag{3.2}$$

where E is the energy, mass is M, subscripts i and t represents the incident particle and target particle respectively and θ is the emission angle or angle of incidence as measured from the line joining their centers of the masses as denoted [15] in Fig. 3.3. The maximum energy is transferred when $\cos\theta = 1$ and $M_i = M_t$ and thus it is very important to match the atomic mass of the incident ion to the target atom.

Incident energy of the ion plays a vital role in sputtering process: at a low incident energy, the particles do not have the energy to break the bonds and result in a small reaction. But with a high incident energy, the bombarding particles deeply drive into the substrate allowing for the sputtering of the atoms. If the mass of the incident ion is less than the mass of the surface atom, it bounces back and if the mass of the incident atom is more than the surface atom then they will direct toward the interior surface. When an ion

approaches the surface with particular amount of energy and bombards at a certain angle, it will be neutralized with the lattice electrons on the surface. This process utilizes two different lattice electrons on the surface, one of the lattice electron captures the ion and gets neutralized while the other electron obtains the excess energy and gets ejected from the surface. This process is known as secondary emission and the electrons are referred to as the secondary electrons.

3. Sputtered atom transfer

The transfer of sputtered atoms from the sputtering process is mainly determined by gas pressure. There are three different modes of transfer of sputtered atoms, namely low pressure, intermediate pressure, and high pressure. At low pressures (below 0.1 mTorr), the mean free path is large and the sputtered atoms have more kinetic energy. Ion beam process enhanced magnetron operates in low pressure mode[14]. In intermediate pressure conditions (between 0.5 mTorr and 30 mTorr), the ions undergo more collisions. Most of the sputtering systems operate in this mode. At high pressure (50 mTorr to 5 Torr), the mean free path is short and due to increased collisions, the particles get thermalized with the background gas.

4. Film growth

The sputtered atoms are ejected from the target and get deposited on the surrounding surfaces. The atoms condense on the substrate as loosely bonded atoms. The rate of atom deposition is influenced by the temperature, the energy of particles during collisions and the substrate material[13]. Atoms with higher energies may evaporate from the substrate

surface. Atoms diffuse into nuclei and nuclei form islands. These islands together form a continuous film.

3.1.2 MAGNETRON SPUTTERING

Magnetron sputtering has been developed rapidly over the last decade. This is mainly due to the increased demand toward high quality functional films. By the suitable application of a magnetic field, electrons can be deflected near the target surface. The appropriate placement of magnets can allow electrons to circulate on the closed path. The most prevalent magnetron source is the planar magnetron where the sputter erosion path is a closed circle on a flat surface. The planar magnetron configuration forms a vaporization source that consists of two parallel lines and the cathode source allows deposition on the inside of the cylinder. The hollow cylindrical configuration will deposit the unused material back on the target so that it can be re-sputtered. Fig. 3.3 shows a typical planar magnetron arrangement.

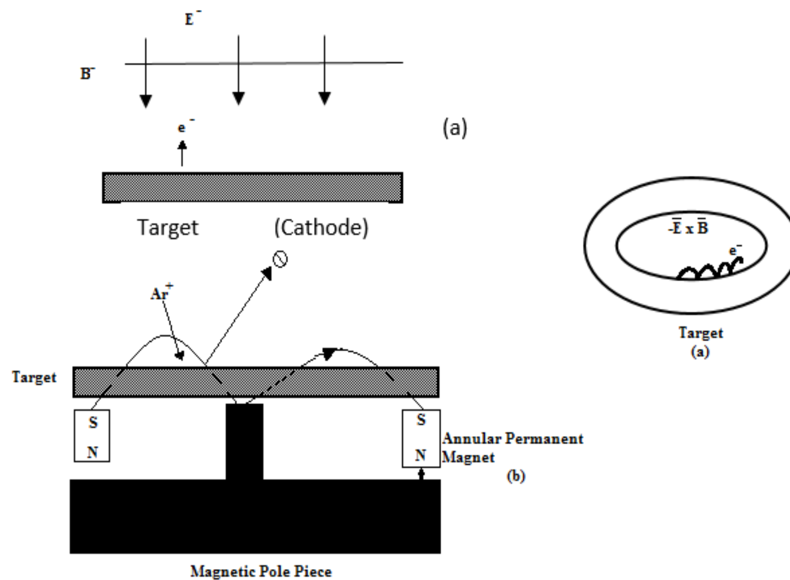

Fig. 3.3 Schematic of a planar magnetron arrangement [based on 13]

The superiority of magnetron sputtering is that it has a high density plasma at low pressures, so that the ions are accelerated without loss of energy resulting in a good sputtering rate with low potential on target[15].

3.1.3 RADIO FREQUENCY (RF) SPUTTERING

In the conventional DC technique, the accelerating potential cannot be directly applied to an insulator surface (as it will charge it), so we use RF sputtering. Fig. 3.4 shows the schematic arrangements for an RF sputtering system with a capacitive, parallel plate discharge. When an RF potential with a very large voltage is capacitively coupled to the electrode, an alternating potential appears on the surface. In the first half cycle, when the applied target voltage is negative, there is negligible amount of current flow due to the low mobility of ions. When voltage alternates positive in the second half cycle, the target becomes positively charged and draws a large electron current due to high electron mobility. The target behaves like a negatively biased cathode and the ion sheath formed in between the target and the gas ions accelerates towards the cathode resulting in sputtering. RF frequencies are used for sputter deposition in the range of 0.5-30 MHz and can perform at low gas pressures (less than 1 mTorr)[16]. Additionally, RF sputtering can be used to sputter electrically insulating materials even though the sputtering rate is low. The major disadvantage of this arrangement is that the RF source is more complicated than a DC source and requires a matching network.

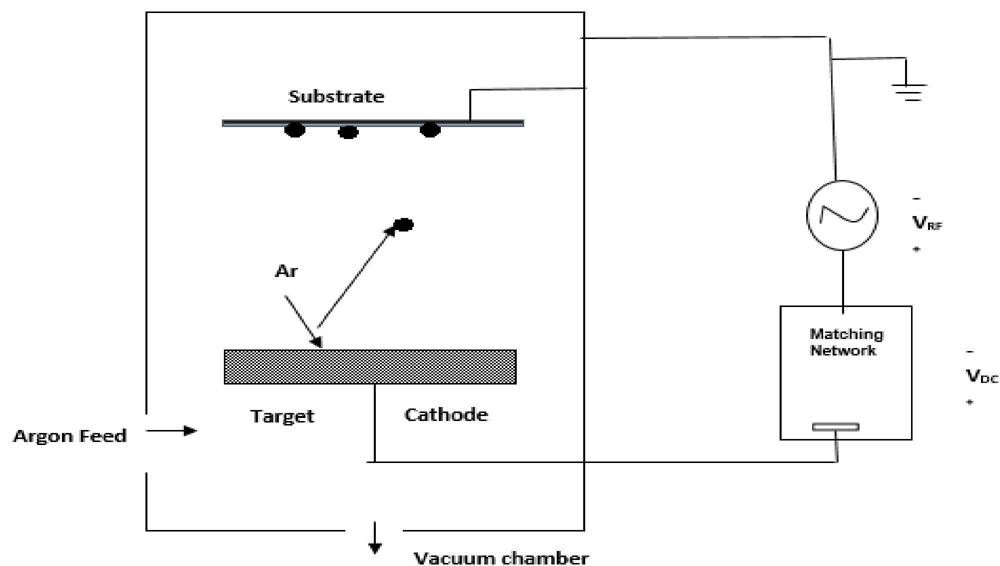

Fig. 3.4 Schematic showing the principal arrangement of a RF sputtering system [based on 13]

3.2 SAMPLE PREPARATION

The P-type doped silicon thin films were prepared by RF magnetron sputtering from a 3” Boron doped p-type silicon target in an argon atmosphere. The deposition process was carried out at base pressure of 4E10^{-7} Torr to reduce the contamination from the atmospheric gas during the loading of the samples. The argon pressure was maintained at 0.5 mTorr for all the depositions. Soda lime glass, quartz, silicon wafers with a native oxide layer and silicon wafers with a thermal oxide layer (500 nm) were used as the substrates. The depositions were carried out at temperatures varying from room temperature to 750 ºC. *Ex-situ* spectroscopic ellipsometry (SE) data were acquired after film growth using a multichannel ellipsometer with a photon energy range of 0.75 to 6.5 eV at angles of incidence of 55°, 65°, and 75°. Complementary characterization of the as-deposited films included x-ray diffraction (XRD) measurements, Hall effect measurements, and resistivity measurements (4-points probe).

3.3 EFFECT OF SUBSTRATE TEMPERATURE

P-type silicon thin films were deposited by sputtering on different substrates at temperatures ranging from room temperature to 750ºC. The complex dielectric functions extracted from SE on Silicon wafer with native oxide are illustrated in Figure 3.5. It can be seen that at temperatures below 600ºC, the silicon layer does not show any feature, indicative of an amorphous layer. For deposition temperatures above 700ºC, several features appear notably between 300-400 nm, indicating that the samples are nano-crystalline.

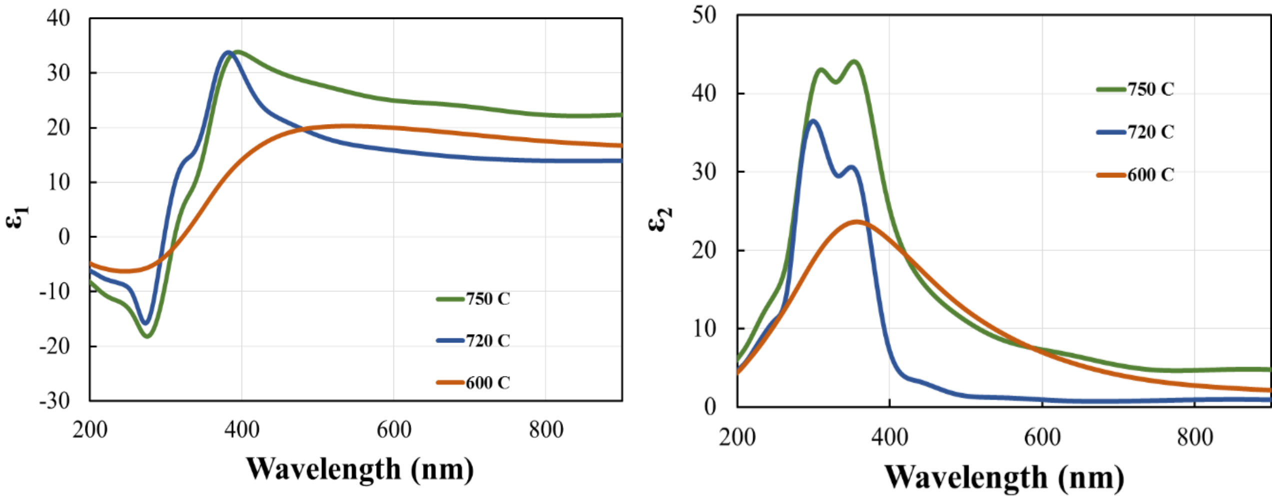

Fig. 3.5 Complex dielectric functions ε_1 and ε_2 extracted by spectroscopic ellipsometry as a function of substrate temperature for silicon thin films deposited on silicon wafers with native oxide.

3.4 EFFECT OF SPUTTERING POWER

In general the structure and the electrical properties of the films strongly depend on the deposition process. Sputtering power during deposition was therefore varied from 200 W to 400 W in 3” target and the effect of the variation of the power was observed on the deposited films. The other deposition parameters such as base pressure, deposition pressure, substrate temperature, and thickness of the films were kept constant for all the deposited films. Figure 3.6 shows the variation

of the XRD spectra for these films deposited at different RF powers. As one can see, there is a definite improvement in the crystallinity of the film with the increase in power. At 200 W, only a broad amorphous peak can be seen around 65º, which correspond to the (400) peak of silicon. As the power increases to 300W, new peaks appear at lower angle, which also correspond

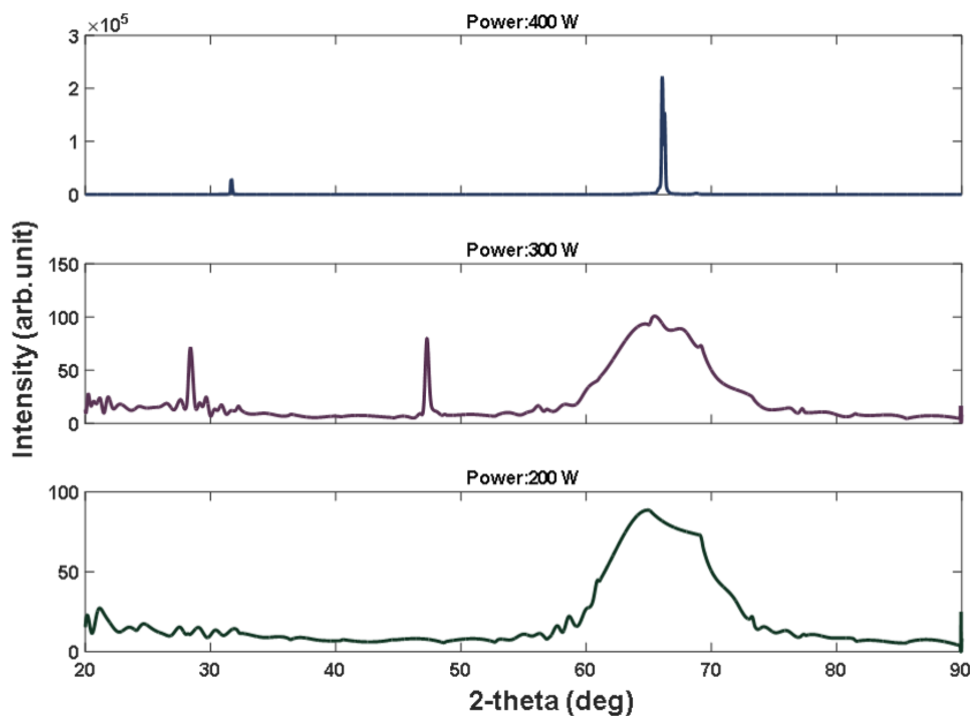

Fig. 3.6 XRD spectra of the deposited silicon film for different sputtering power

to silicon. Finally, at 400W, only two main peaks appear with much higher intensity and reduce full width at half maximum, indicating increase content of crystalline phase as well as increased grain size.

The influence of the RF power on the electrical properties on the silicon film is shown in Figure 3.7. The mobility of the films tends to improve with the increasing sputtering power, indicating higher quality of the films. Overall, the higher sputtering power provides sufficient kinetic energy to the adatoms, improving the surface mobility leading to larger crystallite sizes, which in turns enhanced the electrical properties of the films.

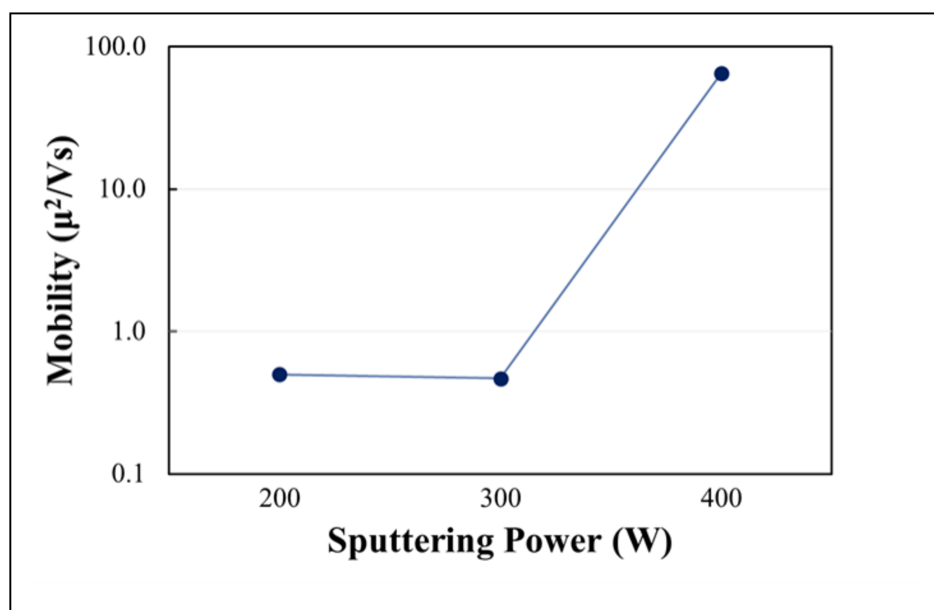

Fig. 3.7 Influence of sputtering power on the electrical mobility of the silicon film.

3.5 EFFECT OF SUBSTRATES

The films were deposited on different substrates – namely quartz, fused silica, silicon wafers with native oxide, as well as silicon wafers with thermal oxide. Quartz and fused silica substrates were chosen for the ease of Hall effect measurements and due to their ability to withstand higher temperatures. The electrical properties were measured mainly for quartz and fused silica

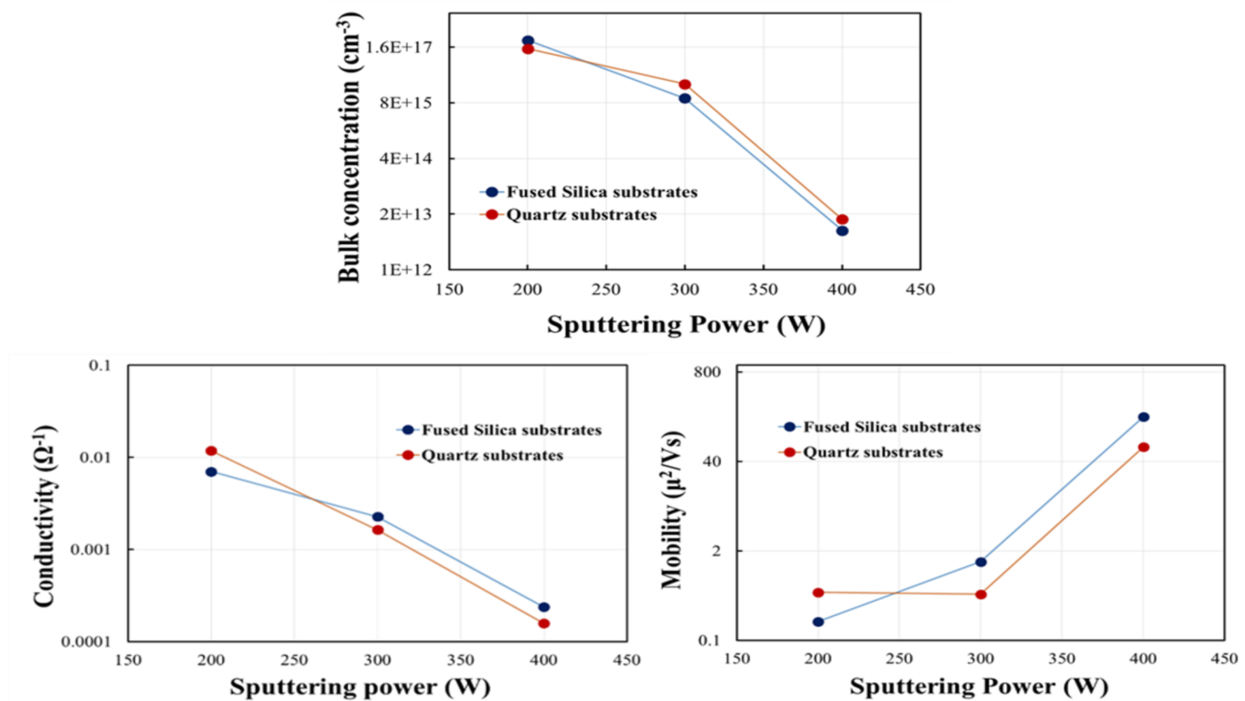

Fig. 3.8 Influence of sputtering power on electrical properties of the silicon films for different substrates

substrates, as chances were high to probe through to the silicon substrates. Figure 3.8 compares the bulk concentration, mobility, and conductivity for the different substrates with a variation of sputtering power. As one can see, there is not a lot of mismatch between the two substrates, indicating little influence of the substrates for that property.

The complex dielectric function ε_2 as extracted from ex-situ SE is shown in Figure 3.9 for different substrates. As one can see, the films deposited on silicon wafers (both native oxide and thermal oxide wafer) have a better crystalline quality. Effectively, the films deposited on quartz and fused silica substrates do not have the signature peaks at 295 nm and 364 nm (4.2 eV and 3.4 eV) and the films are likely amorphous.

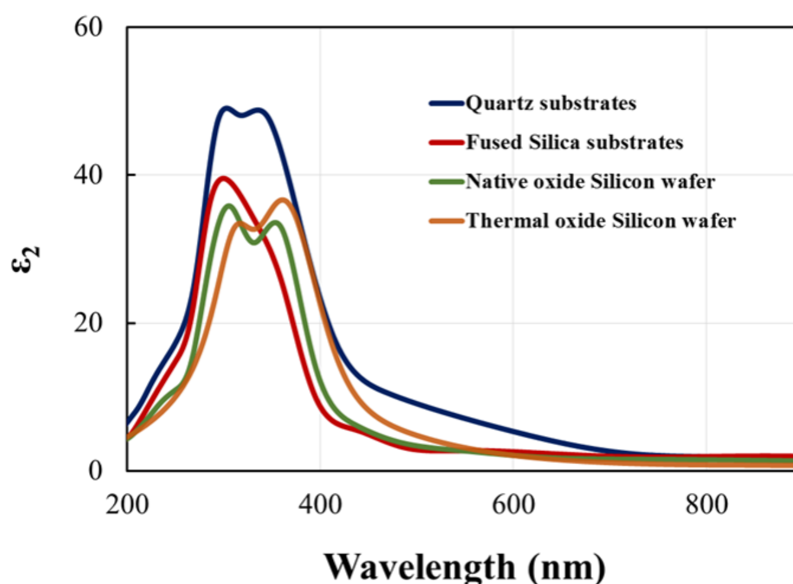

Fig. 3.9 Complex dielectric function ε_2 extracted by spectroscopic ellipsometry for different substrates

The results were compared with the XRD spectra shown in Figure 3.10. It is clear from the XRD spectra that the silicon films deposited on the quartz and fused silica substrates did not crystallize readily. The large peak at low angle shows the background peak from the amorphous glass substrate. For the films deposited on the silicon wafer however, a large peak appears around 66°, due to nanocrystalline silicon. The shift of the peak toward higher angles for the thermal oxide substrate is not explained at this stage.

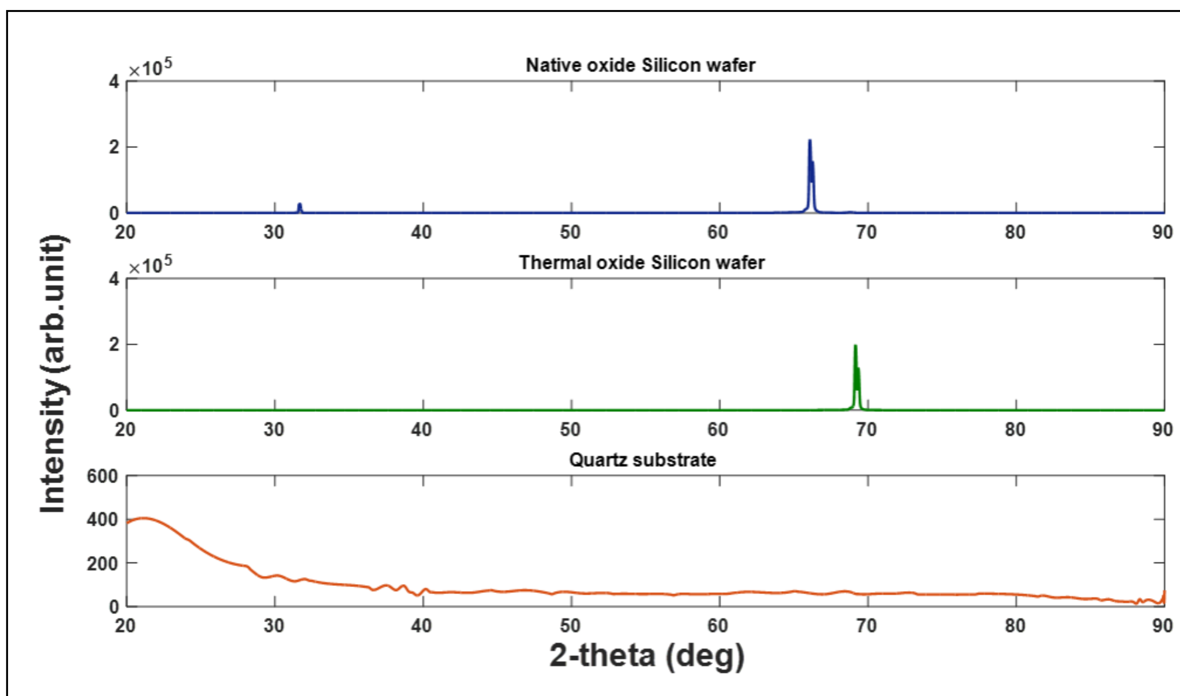

Fig. 3.10 XRD spectra of the deposited silicon film on different substrates

3.6 CONCLUSION

In this chapter, silicon thin films were deposited by rf magnetron sputtering on various substrates. The effect of substrates temperature, sputtering power and substrates were studied. It was observed that a temperature of at least 700ºC, with a power of 400W was necessary to deposit nano-crystalline films. It was also observed that films deposited on silicon wafers led to higher crystalline phase compared to quartz substrates.

CHAPTER 4

EFFECT OF ION BEAM ASSISTED DEPOSITION ON SILICON THIN FILMS GROWTH

Ion beam technology was developed at NASA in the 1960s as a means of producing thrust on spacecraft. In the last decades, thin film deposition evolved into a ubiquitously present technology penetrating all major industries[17]. Ion-assisted deposition has evolved from a collection of individual "recipes" to the use of precise ion energy per deposited atom to allow for enhanced deposition process. Ion beam-assisted deposition, the bombardment of thin film with a beam of energetic particles during deposition provides a powerful technique for modifying the microstructure and properties of thin films such as adhesion, hardness, refractive index, stress, crystalline orientation, resistance to atmospheric degradation, or the selection of certain molecular bonds. The advantage of employing IBAD for the fabrication of thin films is mainly due to the low contamination level from sputter gases and very good control over the properties of thin films.

4.1 ION SOURCES

Earlier applications of ion-assist depositions used gridded ion sources. Moreover, the ion-beam current capacity of gridded sources is limited at low ion energies due to the space-charge limit in the acceleration process, which in turn limits their production processing capability. Gridless ion sources accelerate ions in a quasi-neutral plasma, in such a way that there is no current limit similar to gridded sources and substantial ion currents can be accelerated at low ion energies. Therefore the choice of ion beam portion mainly depends on the desired range of energy. Most of the gridless ion sources used in ion assist applications are of the end-Hall type. The low energy source recently developed for IBAD applications is the end-Hall source. The ion current and ion energy of end-

Hall ion sources are not available from power-supply meters and must be determined from probe surveys of the ion beams. The lower ends of these ranges are more typical of the earlier version of the end-Hall ion source and the higher ends are more typical of the later version. The absence of grids also reduces the maintenance requirements of end-Hall ion sources compared to gridded sources.

4.2 THEORY OF OPERATION

The function of ion beam source is to produce ions and accelerate these ions to high velocities, so they are ejected downstream from the source. The ejected ions are lead to form a "beam" in which the ions are mono-energetic with respective velocities. An ion beam source consists of four (4) key elements: 1) Discharge Chamber; 2) Electron Source; 3) Grids and 4) Neutralizer. Figure 4.1 is a schematic of an ion beam source. A brief, physical description of each of the four elements is presented below.

1. Discharge Chamber: Basically, the source is operated by introducing the source gas into the discharge chamber, in which the source gas is ionized. For DC sources, the discharge

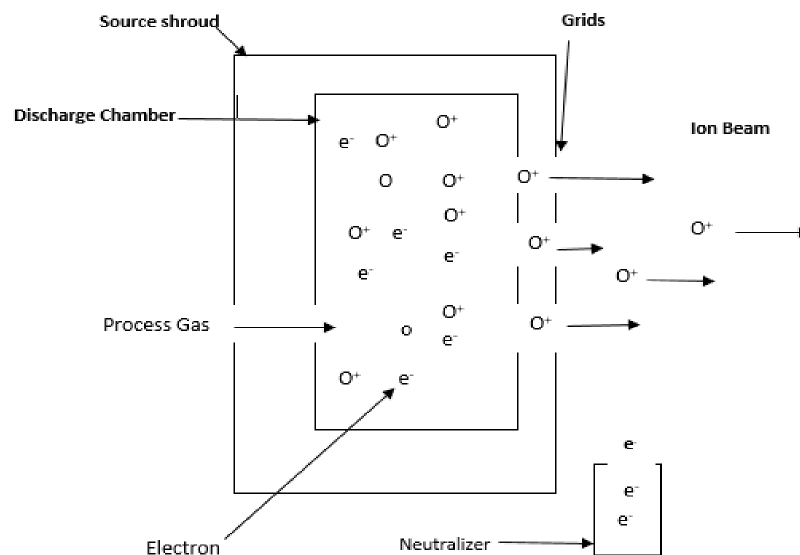

Fig. 4.1 Schematic of an ion beam source [based on 18]

chamber is referred to as the body. The chamber will have a magnetic field produced using permanent magnets. The purpose of the magnetic field is to control the motion of electrons such that they can have various ionizing collisions with the source gas before being collected on the anode.

2. Electron Source: An electron source is used to ionize the gas and establish plasma. Recall, plasma is an electrically conductive gas where the density of ions and electrons are approximately equal. For DC sources, the electron source can be either a hot filament or a hollow cathode. This research uses a source with hot filament. Typically, a filament consists of a tungsten wire which is heated to emit electrons. The electrons from either the filament or a hollow cathode are then used to ionize the source gas. The electrons have several ionizing collisions before being collected at the anode surface in a DC source.

3. Grids: Ions created in the discharge chamber are then accelerated to high velocities with the source grids, the electrostatic apertures by which the ions from the discharge are extracted. Grids are electrodes separated from each other by a few millimeters. Each grid has several apertures that are aligned and allow for the extraction of ions. The grid closest to the discharge chamber is referred to as the screen (or S) grid. Moving downstream, the next grid is referred to the accelerator (or A) grid. On some sources, a third grid is used (which is the furthest downstream from the discharge chamber) and it is referred to as the decelerator (or D) grid. This research uses a three grid system. The grid assembly extracts ions from the discharge chamber by applying specific potentials (or voltages) to each grid. A potential (or voltage) diagram of the ion acceleration process is presented in Figure 4.2. First, the S grid is biased positively (beam voltage) with respect to the ground and consequently the plasma in the discharge chamber is also biased positive with respect to

the ground. Next, the A grid is biased negative (accel voltage) with respect to the ground and establishes an electric field along the source centerline. Positive ions in the discharge chamber that drift close to this electric field are accelerated. Even if the D grid is not used, the potential downstream from the source is ultimately approximately zero. Depicted in Figure 4.2 is the electric potential for a three grid assembly. The D grid potential is typically held at ground potential (or 0 V). The accelerated ions then decelerate after passing the A grid and exit the aperture with a net ion energy of approximate beam voltage. As depicted in Figure 4.2, electrons either located in the discharge chamber or downstream from the source are separated due to the established electric field. Ions extracted through

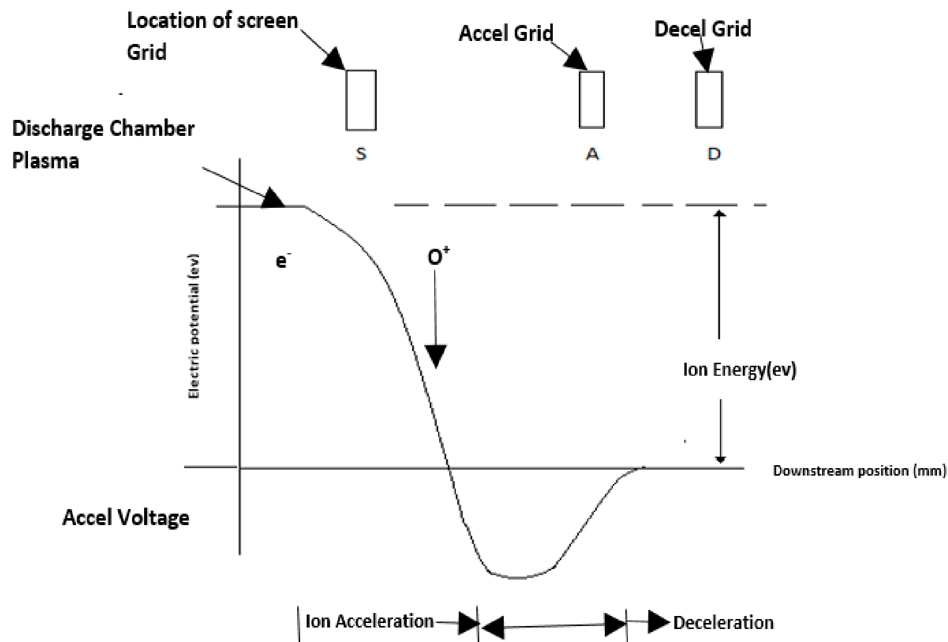

Fig. 4.2. Schematic of the ion acceleration process [based on 18]

the grid apertures comprise individual beamlets and a typical grid assembly will have numerous apertures. As a result, individual beamlets combine to form a more, broad ion beam.

4. Neutralizer: A neutralizer is set downstream from the ion beam source where it produces electrons to adjust the amount of positive particles, which leave the source. The emitted electrons provide a charge balance for the ions leaving the source. For DC sources, the neutralizer can be a hot filament, hollow cathode, or plasma bridge type. A plasma bridge neutralizer (PBN) is where a hot filament is placed in a smaller discharge chamber through which an inert process gas is supplied. Normally, a larger number of electrons is discharged from the neutralizer rather than particles from the source. This is done to limit and additionally dispose of the space or surface charging that may happen. In most situations, electrons from the neutralizer do not directly combine with the ions in the beam to form high energy neutrals.

4.2.1 EXPERIMENTAL SETUP

The ion beam source requires a power supplies. In Fig 4.3, the electrical connections for a filament cathode and filament neutralizer DC source are presented. The cathode is heated using an AC control power supply. Electrons leaving the filament are collected at the anode with the discharge supply, a DC bias supply. The beam supply, also a DC bias supply, is connected to the anode and biases the discharge plasma positive with respect to ground. Not illustrated, but normally used, is a resistor placed between the body and anode. The body resistor establishes the proper bias between the anode and body and thereby directs electrons to be collected on the anode surface. The accelerator supply, a DC type supply, biases the accel grid negative with respect to ground. Finally, the neutralizer filament is heated using an AC power supply.

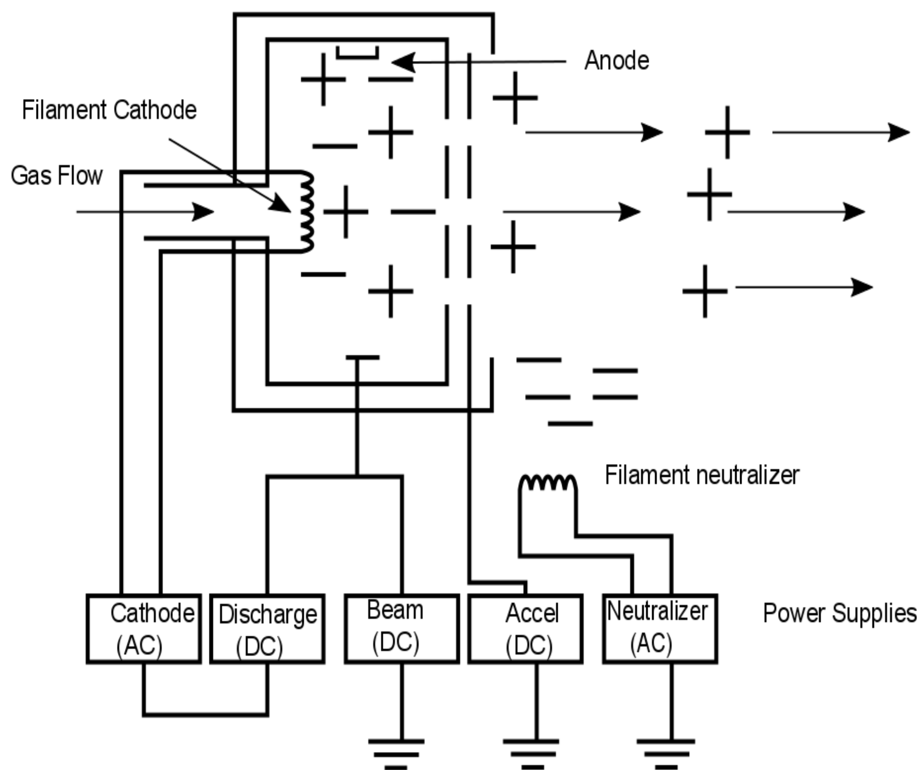

Fig. 4.3 The electrical schematic for a filament DC source [based on 18]

4.3 SAMPLE PREPARATION

P-type doped silicon thin films were prepared by RF sputtering from a 3” Boron-doped p-type silicon target in an argon atmosphere. The deposition process was carried out at base pressure of $4E10^{-7}$ Torr to reduce the contamination from the atmospheric gas during the loading of the samples. The argon pressure was maintained at 0.5 mTorr for all the depositions. Soda lime glass, quartz, silicon wafers with a native oxide layer, and silicon wafers with a thermal oxide layer (500 nm) were used as the substrates. The depositions were carried out at temperatures varying from room temperature to 750 ºC. *Ex-situ* spectroscopic ellipsometry (SE) data were acquired after film growth using a multichannel ellipsometer with a photon energy range of 0.75 to 6.5 eV at angles of incidence of 55°, 65°, and 75°. Complementary characterization of the as-deposited films

included x-ray diffraction (XRD) measurements, Hall effect measurements and resistivity measurements (four point probe).

4.4 EFFECT OF ION BEAM PARAMETERS

Figure 4.4 illustrates the influence of ion beam on the deposition of thin film silicon, by looking at the evolution of the dielectric functions. The other sputtering deposition parameters were kept constant. One can see a clear transition from amorphous phase without IBAD to crystalline films with IBAD.

The mobility of surface and near surface atoms can be controlled during the growth surface using a low energy ion beam. The beam voltage was varied from 35 V to 400 V and the maximum ion current was fixed for a constant beam voltage to avoid direct impingement of the energetic ions. As shown in Figure 4.5, higher mobilities were obtained at a low ion energy (100 eV) and ion beam current of 3 mA. An increase in the ion energy above 250 – 300 eV resulted in the etching of the films. On the other hand, a combination of low ion energy and low ion beam current proved to lead to film with higher conductivity, as shown in Figure 4.6.

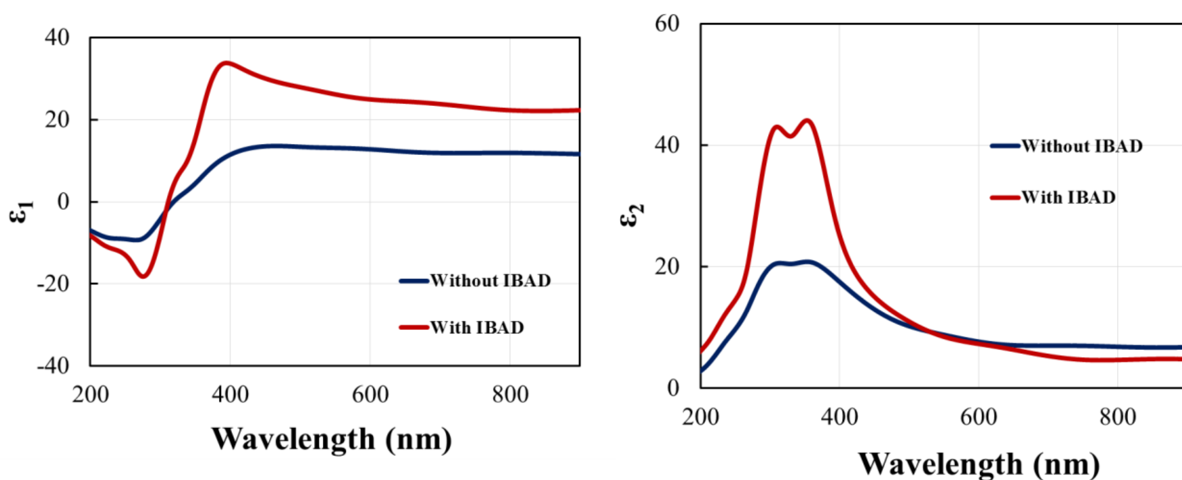

Fig. 4.4 Influence of ion beam on the optical properties of the sputtered silicon films extracted by spectroscopic ellipsometry

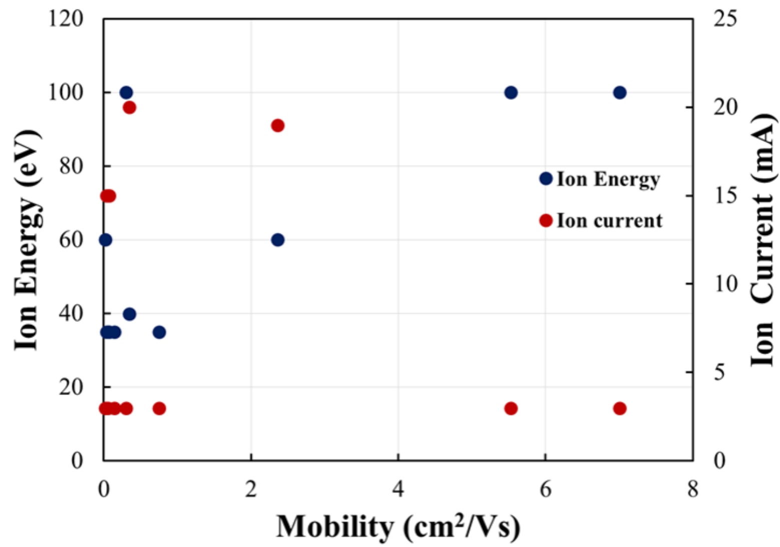

Fig. 4.5 Influence of ion beam parameters on the mobility of the silicon films

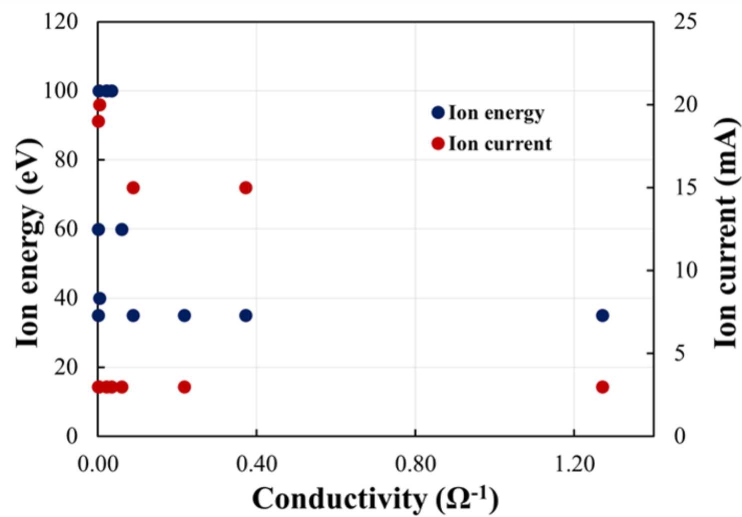

Fig. 4.6 Influence of ion beam parameters on the conductivity of the silicon films

4.5 EFFECT OF SPUTTERING POWER

In order to study the effect of sputtering power on the crystallinity of silicon films, the sputtering power during deposition was varied from 200 W to 450 W. The other deposition parameters such as base pressure, deposition pressure, substrate temperature, ion beam parameters, and thickness of the film were maintained constant. Figure 4.7 shows the variation of the complex dielectric functions ε_1 and ε_2 as obtained by SE for different sputtering power. As one can see, there is a clear improvement in the crystallinity of the film with the increase in the power. This was confirmed by analyzing the XRD spectra for the same powers (Figure 4.8). As one can see, the films at 200W are amorphous to nanocrystalline with only a broad peak around 66°. As the power increases, the peak reduces in broadening and a clear peak appears with smaller full width at half maximum, indicative of larger crystallites. At 450W, only one peak appears indicating the polycrystalline nature of the film.

With the increase in the sputtering power along with IBAD, the surface adatoms are provided with higher kinetic energy and the nucleation and the growth of the film is enhanced. In the low energy regime of ion beam, the grain boundaries of the films can easily be moved and thus the films show larger crystallite sizes with higher RF power and low ion beam energy. The silicon film deposited at 450 W can be clearly identified to be a polycrystalline film.

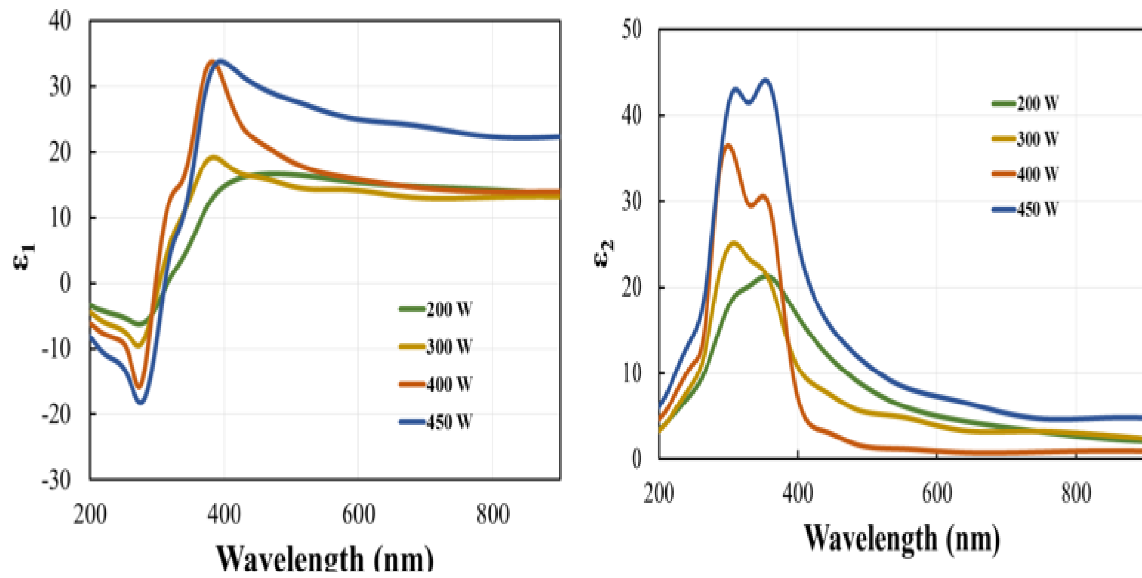

Fig. 4.7 Complex dielectric function spectra ε1 and ε2 of silicon films deposited with IBAD as a function of sputtering power

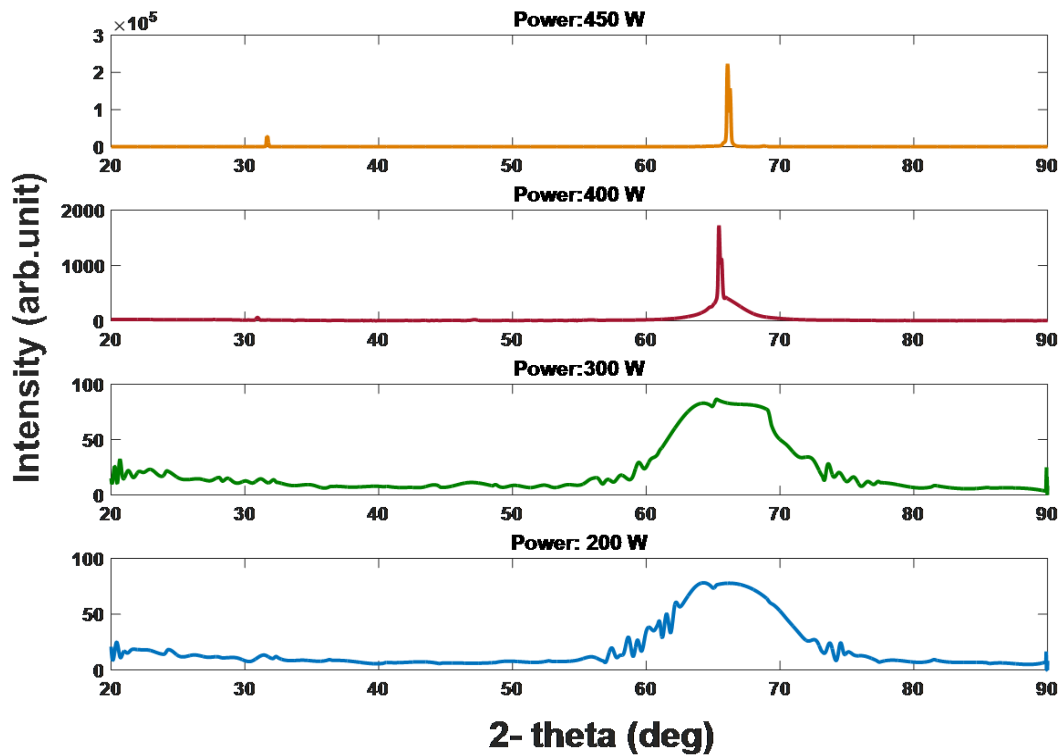

Fig.4.8. XRD spectra of IBAD deposited silicon film for different sputtering powers

4.6 CONCLUSION

In this chapter, silicon thin films were deposited by rf magnetron sputtering with the addition of an ion beam. The effect of having an ion beam and the sputtering power were studied. It was clearly shown that having an ion beam greatly enhanced the crystallinity of the films. Specifically, a lower beam voltage lead to better films. Once an ion beam is present, increasing the sputtering power yield to higher quality films in terms of crystallinity.

CHAPTER 5

SUMMARY

5.1 SUMMARY

This thesis examines modifying the deposition process of silicon thin films, by using a combination of sputtering and ion beam deposition. Various substrates were used, including soda lime glass, quartz, silicon wafers with a native oxide layer and silicon wafers with a thermal oxide layer (500 nm). The depositions were carried out at temperatures varying from room temperature to 750 ºC, power ranging from 100 W to 450 W, and beam voltage varying from 35 V to 400 V. Characterizations of the as-deposited films included spectroscopic ellipsometry, x-ray diffraction (XRD) measurements, Hall effect measurements, and resistivity measurements (four point probe).

Silicon thin films were deposited by rf magnetron sputtering on various substrates. The effect of substrates temperature, sputtering power, and substrates was studied. It was observed that a temperature of at least 700ºC, with a power of 400W was necessary to deposit nano-crystalline films. It was also observed that films deposited on silicon wafers lead to higher crystalline phase compared to quartz substrates.

Silicon thin films were also deposited by a rf magnetron sputtering with the addition of an ion beam. The effect of having an ion beam and the sputtering power was studied. It was clearly shown that having an ion beam greatly enhanced the crystallinity of the films. Specifically, lower beam voltage lead to better films. Increasing the sputtering the power in the presence of an ion beam, yield to higher quality nano-crystalline films.

5.2 FUTURE WORK

Future work includes implementing this deposition process while passivating grain boundaries with hydrogen, producing thin films at reasonably high deposition rates, and also to effectively implement these layers into PV test structures.

REFERENCES

[1] D. M. Chapin, C. Fuller, and G. Pearson, "A new silicon p-n junction photocell for converting solar radiation into electrical power," *Journal of Applied Physics,* vol. 25, no. 5, pp. 676-677, 1954.

[2] M. A. Green *et al.*, "Solar cell efficiency tables (version 49)," *Progress in Photovoltaics: Research and Applications,* vol. 25, no. 1, pp. 3-13, 2017.

[3] M. G. Deceglie, "Advanced silicon solar cell device physics and design," Citeseer, 2013.

[4] T. Saga, "Advances in crystalline silicon solar cell technology for industrial mass production," *NPG Asia Mater,* vol. 2, pp. 96-102, 07/22/online 2010.

[5] M. Taguchi *et al.*, "24.7% Record efficiency HIT solar cell on thin silicon wafer," *IEEE Journal of Photovoltaics,* vol. 4, no. 1, pp. 96-99, 2014.

[6] E. V. Kerschaver and G. Beaucarne, "Back-contact solar cells: A review," *Progress in Photovoltaics: Research and Applications,* vol. 14, no. 2, pp. 107-123, 2006.

[7] A. F. B. Braga, S. P. Moreira, P. R. Zampieri, J. M. G. Bacchin, and P. R. Mei, "New processes for the production of solar-grade polycrystalline silicon: A review," *Solar Energy Materials and Solar Cells,* vol. 92, no. 4, pp. 418-424, 4// 2008.

[8] (2016). *Advanced characterization techniques for thin film solar cells*. Available: http://dx.doi.org/10.1002/9783527699025

[9] J. Schuttauf, "Amorphous and crystalline silicon based heterojunction solar cells," Utrecht University, 2011.

[10] H. Fujiwara, *Spectroscopic ellipsometry: Principles and applications*. Wiley, 2007.

[11] S. M. Sze and K. K. Ng, *Physics of semiconductor devices*. John Wiley & Sons, 2006.

[12] P. M. Martin, *Handbook of deposition technologies for films and coatings: Science, applications and technology*. William Andrew, 2009.

[13] K. Wasa, M. Kitabatake, and H. Adachi, *Thin film materials technology: Sputtering of control compound materials*. Springer Science & Business Media, 2004.

[14] N. Williams and J. Cuomo, "Sputter deposition," *Wiley Encyclopedia of Electrical and Electronics Engineering,* 2003.

[15] R. V. Stuart, *Vacuum technology, thin films, and sputtering: An introduction*. Academic Press, 2012.

[16] D. M. Mattox, *Handbook of physical vapor deposition (PVD) processing*. William Andrew, 2010.

[17] M. D. Rayman and P. Varghese, "The Deep Space 1 extended mission," *Acta Astronautica,* vol. 48, no. 5, pp. 693-705, 2001.

[18] Kaufman, H.R., R.S. Robinson, "*Broad-beam ion sources*," Handbook of Plasma Processing Technology, pp. 183-193, Noyes Pub., New Jersey, 1990.

VITA

Tejaswini Miryala

231 Kaufman Hall
ECE Department
Old Dominion University
Norfolk, VA 23529

Education

2017	**M.S.**	Electrical & Computer Engineering	Old Dominion University, VA
2015	**B.TECH**.	Electrical & Electronics Engineering	JNTU Hyderabad, India